Velocity measurements in confined swirling flow of polymer solutions with vortex shedding

Shinji Tamano,[a] Motoyuki Itoh, Yuichiro Ide, and Kazuhiko Yokota
Graduate School of Engineering, Nagoya Institute of Technology, Gokiso-cho, Showa-ku, Nagoya, Aichi 466-8555, Japan

(Received 28 February 2007; accepted 6 June 2007; published online 20 August 2007)

A particle image velocimetry system is used to examine the velocity field in the unsteady swirling flow of polyacrylamide (PAA) solutions (PAA 0.5 wt. % and 1.0 wt. %) with the vortex shedding due to a rotating disk in a cylindrical casing. In our earlier work [Tamano *et al.*, Phys. Fluids **19**, 023103 (2007)], the vortex shedding is investigated by the flow visualization technique. In this work, we investigate the velocity field for better understanding of the vortex shedding mechanism and the nonaxisymmetric ring vortex which was observed for the higher Reynolds number compared to that of the axisymmetric ring vortex. It was found that the fluid within the ring vortex formed near the rotating disk rotates with semirigid rotation, where the angular velocity of the ring vortex was about 0.9 times that of the rotating disk. A high shear layer existed at the boundary between the ring vortex and the outer large-scale secondary flow. When the ring vortex was shed, the surrounding large-scale secondary flow rushed into near the rotating axis, so that strong axial flow was observed near the rotating axis. For the nonaxisymmetric ring vortex, azimuthal and radial velocities oscillate periodically with considerably large amplitude. In addition, the joint probability density function showed that the correlation between azimuthal and radial velocity fluctuations varied with the radial locations. © *2007 American Institute of Physics*. [DOI: 10.1063/1.2754246]

I. INTRODUCTION

The swirling flow of viscoelastic fluids in an enclosed cylindrical casing with a rotating bottom lid is commonly encountered in many process engineering applications. It has been reported that the confined swirling flow field of viscoelastic fluids is considerably complex compared to that of Newtonian fluids. Hill[1] first reported that the secondary flow direction of polyacrylamide solutions due to a rotating disk in a cylindrical casing was opposite to that of Newtonian fluids due to the elastic force. Day *et al.*[2] observed the formation of the ring vortex near the center of the rotating disk in aqueous polyacrylamide solutions and the highly unsteady flow pattern in the half of the cylinder closest to the rotating lid, and then introduced the elastic number, which was the ratio of elastic to viscous time scales or the ratio of the elastic to inertial forces, in order to categorize the secondary flow patterns. Escudier and Cullen[3] observed the double cell structure of the secondary flow of highly shear-thinning carboxymethylcellulose solutions with the elastic number relatively small using flow visualization technique. Recently, Moroi *et al.*[4] and Itoh *et al.*[5] have investigated velocity fields of the confined swirling flow of aqueous polyacrylamide solutions using particle tracking velocimetry (PTV) and laser Doppler velocimetry (LDV) measurements, respectively. Moreover, Stokes *et al.*[6,7] performed particle image velocimetry (PIV) measurements of confined swirling flows of a range of low-to high-viscosity flexible polyacrylamide solutions with a constant viscosity (Boger fluids) and a semirigid xanthan gum Boger fluid, and clarified the inertia and elasticity effects on velocity fields. The previous studies on the confined swirling flow of viscoelastic fluids are reviewed in the comprehensive studies of Stokes *et al.*[6,7]

However, there have been fewer studies on unsteady confined swirling flows of viscoelastic fluids at relatively high Reynolds number than on steady swirling flows. Recently, Stokes and Boger[8] investigated unsteady (chaotic) secondary flow using flow visualization, and presented a stability boundary diagram for the confined swirling flow of polyacrylamide Boger fluids. Quite recently, Tamano *et al.*[9] found a vortex shedding phenomenon in the confined swirling flow of aqueous polyacrylamide solutions with a shear-thinning property. Figure 1 shows the pictorial representation of typical flow fields with the vortex shedding observed by three-dimensional flow visualization.[9] The vortex shedding phenomenon is briefly explained as follows. After the onset, the ring vortex gradually becomes larger with time, and leads to a quasisteady state [Fig. 1(a)]. Sometime later, the ring vortex moved away from the rotating disk with time [Fig. 1(b)]. Then the ring vortex was involved in the background secondary flow near the center of the cylinder, and finally disappeared. Tamano *et al.*[9] also proposed a possible vortex shedding mechanism based on elastic energy, in which the ring vortex is shed away from the rotating disk to release the elastic energy stored inside the ring vortex due to the elastic force, when the amount of its energy exceeds a critical value. In addition, they showed that the ring vortex became nonaxisymmetric at a higher Reynolds number. However, the vortex shedding mechanism and the nonaxisymmetric ring vortex have not been well understood.

PIV measurement, which does not disturb flow fields,

[a]Author to whom correspondence should be addressed. Telephone: +81 52 735 5609. Fax: +81 52 735 5247. Electronic mail: tamano.shinji@nitech.ac.jp

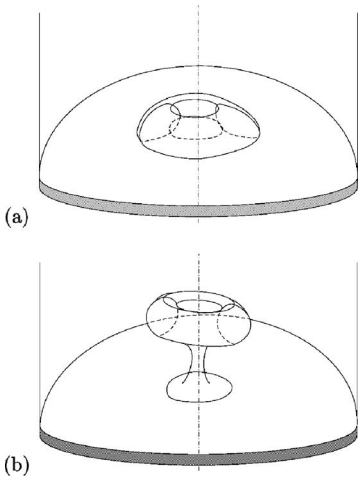

FIG. 1. Pictorial representation of typical flow fields with vortex shedding: (a) formation of ring vortex, (b) vortex shedding.

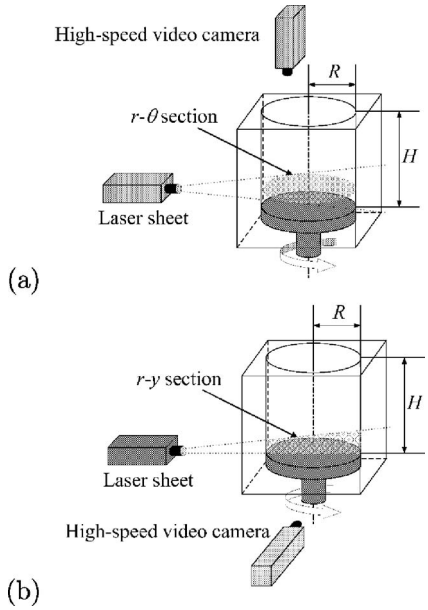

FIG. 2. PIV measurement method: (a) $r-\theta$ section, (b) $r-y$ section.

has now become a helpful tool for understanding the unsteady behavior of the confined swirling flow of Newtonian fluids,[10] but there have been few studies on PIV measurements of the confined swirling flow of viscoelastic solutions such as polymer and surfactant solutions (see Stokes *et al.*[6,7]). Quite recently, Wei *et al.*[11] and Li *et al.*[12] have investigated a swirling flow of dilute surfactant solutions with free surface due to a rotating disk using PIV. However, PIV measurement of unsteady confined swirling flow of polymer solutions with vortex shedding has not been conducted.

In this study, two-dimensional PIV measurements were conducted for better understanding of unsteady swirling flow with vortex shedding. In Sec. II, we present the experimental apparatus and procedure. The mean velocity profiles for the axisymmetric ring vortex are investigated in Sec. III A. Then, the phenomenon of vortex shedding is discussed in Sec. III B. In addition, Sec. III C describes the velocity fluctuations for the nonaxisymmetric ring vortex. Finally, the main conclusions in this study are presented in Sec. IV.

II. EXPERIMENTAL APPARATUS AND PROCEDURE

The present experimental apparatus mainly consists of a rotating disk enclosed in a casing.[9] The surface of the rotating disk is smooth, and the outside diameter is 180 mm (R =90 mm). The aspect ratio of the distance H between the casing end wall and the rotating disk to the radius of the rotating disk R was fixed at $H/R=2.0$. The disk is driven by a motor and decelerator with an inverter control. The inside of the clear acrylic casing is cylindrical, and the outside is rectangular to minimize the effect of light refraction while observing cross sections. The inner diameter of the casing is 181 mm and the outer length on one side is 215 mm. In this study, r, θ, and y represent the radial, azimuthal, and axial directions, and their origin is at the center of the lower rotating disk. The working fluids were polymer solutions of polyacrylamide (Sanfloc AH70P, molecular weight of two to four millions, Sanyo Kasei Kogyo, Ltd.) which was dissolved in tap water and was gently mixed by hand to prevent degradation. The concentrations of polyacrylamide solutions were 0.5 and 1.0 wt. %, in which the elastic numbers $E_0=\lambda\eta_0/(\rho R^2)$ were 14 and 78, respectively. Here, η_0 is the zero shear viscosity of solutions, λ is the relaxation time, and ρ is the density. Readers are referred to the related study[9] in terms of rheological properties of the working fluids tested.

As shown in Fig. 2, two-dimensional PIV measurements were conducted for $r-\theta$ and $r-y$ sections which were illuminated by a laser sheet (Green Laser 50MG Seat, output: 50 mW, wavelength: 532 nm, slit width: 3 mm, Katoukouken, Ltd.), and images on $r-\theta$ and $r-y$ sections were captured by a high speed camera (VCC-H1000, Dejimo, Ltd.) from the upper and side positions of the cylinder, respectively. Frame rates were 125 fps and 50 fps for $r-\theta$ and $r-y$ sections, respectively. The high-speed camera has a resolution of 512×472 pixels. Shutter speed was set at 1/250 s. The flow was seeded with particles (Orgasol2002 ES4 NAT3, mean diameter: 40 μm, specific gravity: 1.03, Arkema, Ltd.). In the present study, we used the original PIV program based on the direct correlation method to obtain the velocity vector field. The erroneous velocity vectors that lay outside a specified range were removed. In order to validate the present PIV measurements, we performed the PIV measurements on $r-\theta$ and $r-y$ sections for the confined swirling flow of a glycerol-water mixture (98 wt. %), and compared experimental data with the corresponding numerical data obtained by the axisymmetric numerical simulation for Newtonian fluids (not shown here).

III. RESULTS AND DISCUSSION

A. Axisymmetric ring vortex

Figures 3(a) and 3(b) show radial distributions of mean azimuthal velocity $V_\theta/(R\Omega)$ and radial velocity $V_r/(R\Omega)$ obtained by PIV measurement on the $r-\theta$ section at the axial

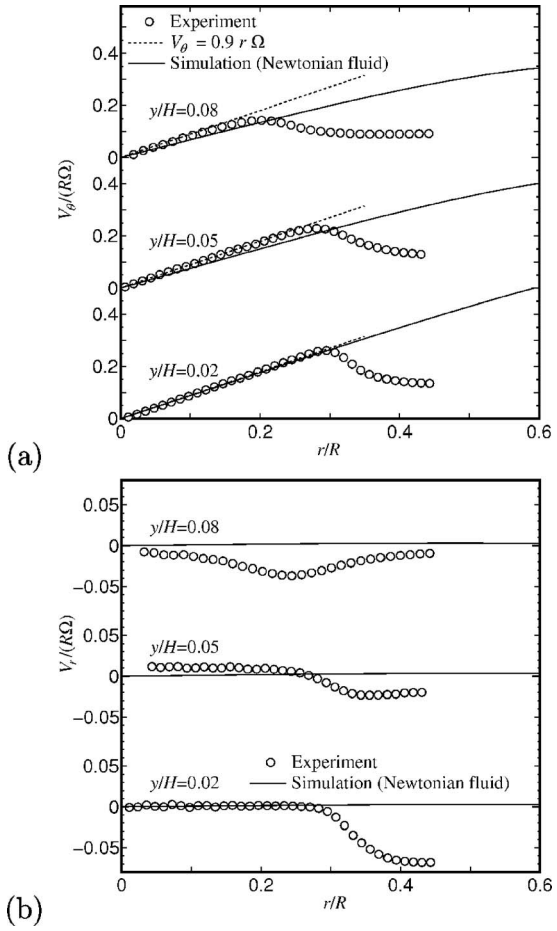

FIG. 3. Radial distributions of mean velocities for PAA 0.5 wt. % at $Re_0=2.1$, $E_0=14$: (a) azimuthal, (b) radial.

locations $y/H=0.02, 0.05, 0.08$ for PAA 0.5 wt. % at Reynolds number $Re_0=2.1$. The Reynolds number Re_0 is defined as follows:

$$Re_0 = \frac{\rho R^2 \Omega}{\eta_0}, \tag{1}$$

where Ω is the angular velocity of the rotating disk. For PAA 0.5 wt. % at $Re_0=2.1$, the typical axisymmetric ring vortex is formed near the center of the rotating disk.[9] The mean velocity is obtained by the time average for $0.5<t/T<0.7$, where t is the time and T is the period for the vortex shedding. In this study, the time when the circulation $\Gamma=0$ defined by Eq. (2) corresponds to $t/T=0$ or 1, which indicates the exact time of vortex shedding (Sec. III B in detail). From some flow visualization results and PIV measurements for PAA 0.5 wt. % at $Re_0=2.1$, it is confirmed that the axisymmetric ring vortex becomes quasisteady for $0.5<t/T<0.7$. In Fig. 3, the experimental data were presented only for $r/R<0.45$ due to the limitation of the resolution of the high-speed camera used. In the figures, solid lines represent data of the axisymmetric numerical simulation[5] for Newtonian fluids at the corresponding Reynolds number.

At the axial locations of $y/H=0.02, 0.05$, for $r/R<0.30$ within the axisymmetric ring vortex, the mean azimuthal velocity follows the relation of $V_\theta=0.9\, r\Omega$ [dotted line in Fig. 3(a)], and the mean radial velocity is almost zero [Fig. 3(b)], which indicates that the fluid within the axisymmetric ring vortex rotates with semirigid rotation, where the angular velocity is about 0.9 times that of the rotating disk. Here, $V_r/(R\Omega)$ at $y/H=0.05$ is slightly positive in the region $0<r/R<0.30$, which indicates that the fluid is flowing slightly outward in the radial direction. This corresponds to the fact that the circulating flow within the ring vortex is outward near the rotating disk and inward away from the rotating disk. The existence of circulation within the ring vortex is also supported by the flow visualization.[9] On the other hand, at $y/H=0.08$, the region in which the relation of $V_\theta=0.9\, r\Omega$ and $V_r\simeq 0$ $(r/R<0.10)$ holds, is much narrower than those $(r/R<0.30)$ at $y/H=0.02, 0.05$, which indicates that the region of the semirigid rotation is only for $r/R<0.10$ at $y/H=0.08$.

At $y/H=0.02, 0.05$, in the region outside of the semirigid rotation $(0.30<r/R<0.50)$, the mean azimuthal velocity is much smaller than that for Newtonian fluids [Fig. 3(a)]. This is due to the shear-thinning property. The same tendency has been observed in the previous study[4] at the lower Reynolds number. The mean radial inward velocity $V_r/(R\Omega)$ suddenly becomes larger in the region $0.30<r/R<0.40$, compared to Newtonian fluids, and becomes almost constant at $r/R\simeq 0.40$ [Fig. 3(b)]. The mean azimuthal velocity $V_\theta/(R\Omega)$ also drastically decreases in the region $0.30<r/R<0.40$ [Fig. 3(a)]. Therefore, it is known that a high shear layer exists in the region $0.30<r/R<0.40$, which corresponds to the boundary between the ring vortex and the outer large-scale secondary flow. The absolute mean radial velocity $|V_r|/(R\Omega)$, $V_r<0$, at $r/R\simeq 0.40$ is much larger than that for $r/R\leqslant 0.30$, which indicates that the radial velocity of the large-scale secondary flow outside the ring vortex is much larger than that within it. Note that the radial velocity is much smaller than the azimuthal velocity. On the other hand, at $y/H=0.08$, the mean radial velocity $V_r/(R\Omega)$ is negative at any radial locations examined, which indicates that the fluid is flowing radially inward, and reaches a minimum at $r/R\simeq 0.25$ [Fig. 3(b)]. The strong inward flow at $y/H=0.08$ in the radial direction is due to the large-scale secondary flows outside the axisymmetric ring vortex.

In the related work,[9] we proposed the mechanism of the vortex shedding as follows. Owing to the large first normal stress difference generated by the high shear layer, an elastic energy may be stored inside the ring vortex near the rotating disk. Eventually, the ring vortex is shed away from the rotating disk to release its energy, when the amount of elastic energy stored inside the ring vortex exceeds a critical value. The existence of the high shear layer clarified by the present investigation supports the vortex shedding mechanism based on the elastic energy.

B. Vortex shedding

Figure 4 shows the time variation of circulation Γ before and after the vortex shedding for PAA 0.5 wt. % at $Re_0=2.1$. The circulation Γ around a closed curve S for the region of $0\leqslant r/R\leqslant 0.30$ and $0.02\leqslant y/H\leqslant 0.20$ including the ring vortex was defined by

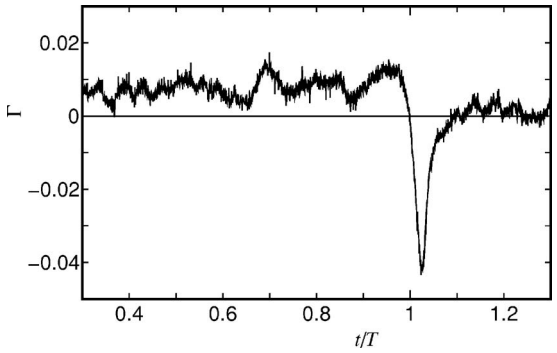

FIG. 4. Circulation fluctuation enclosing the region of $0 \leqslant r/R \leqslant 0.30$ and $0.02 \leqslant y/H \leqslant 0.20$ for PAA 0.5 wt. % at $\mathrm{Re}_0=2.1$, $E_0=14$.

$$\Gamma = \oint_S \left[\frac{v_r}{R\Omega} d\left(\frac{r}{R}\right) + \frac{v_y}{R\Omega} d\left(\frac{y}{H}\right) \right], \tag{2}$$

where the counterclockwise integral is positive. In Fig. 4, the time variation of Γ was presented only for $0.3 < t/T < 1.3$ due to the limitation of the memory size of the high-speed camera used. Before the vortex shedding $(t/T<1)$, the circulation is positive. This is due to the large-scale secondary flow outside the ring vortex. After the vortex shedding $(t/T>1)$, the circulation becomes negative. This is attributable to the fact that the large-scale secondary flow outside the ring vortex is rushed into near the rotating axis [see also Fig. 5(c)]. Note that the levels of Γ are different before and after the vortex shedding, since the period of each vortex shedding is different from the averaged period (see Tamano *et al.*[9]).

Figure 5 shows the velocity vector (black arrows) and contour of $(v_r^2+v_y^2)^{0.5}/(R\Omega)$ in the region $0 \leqslant r/R \leqslant 0.44$ and $0.01 \leqslant y/H \leqslant 0.22$ in the meridian section for PAA 0.5 wt. %, $\mathrm{Re}_0=2.1$. The black and white contours represent large and small nondimensional velocity regions, respectively. Before the vortex shedding $(t/T<1)$, the ring vortex is observed near the rotating disk and the high shear layer exists at the boundary between the ring vortex and the outer large-scale secondary flow [Fig. 5(a)]. At $t/T=1$, the circulating flow almost disappears [Fig. 5(b)]. Just after the vortex shedding $(t/T>1)$, the surrounding large-scale secondary flow rushes into the area near the rotating axis, which is why strong axial flow is observed nearby [Fig. 5(c)].

Figures 6(a) and 6(b) show the axial and radial velocity fluctuations for PAA 0.5 wt. % at $y/H=0.08$, $\mathrm{Re}_0=2.1$. At the location $r/R=0.10$, which corresponds to the inside of the ring vortex, the axial velocity fluctuation $v_y/(R\Omega)$ is almost zero before the vortex shedding $(t/T<1)$, becomes larger after the shedding $(t/T>1)$, and reaches a positive maximum at $t/T=1.024$, due to the strong axial flow away from the rotating disk [Fig. 6(a)]. On the other hand, at the location $r/R=0.40$, which corresponds to the outside of the ring vortex, the axial velocity fluctuation is less affected by the vortex shedding. The negative radial velocity fluctuation $v_r/(R\Omega)$ at $r/R=0.10$ becomes slightly larger after the vortex shedding and becomes minimum at $t/T=1.024$, while $v_r/(R\Omega)$ at $r/R=0.40$ is less affected before and after the vortex shedding [Fig. 6(b)].

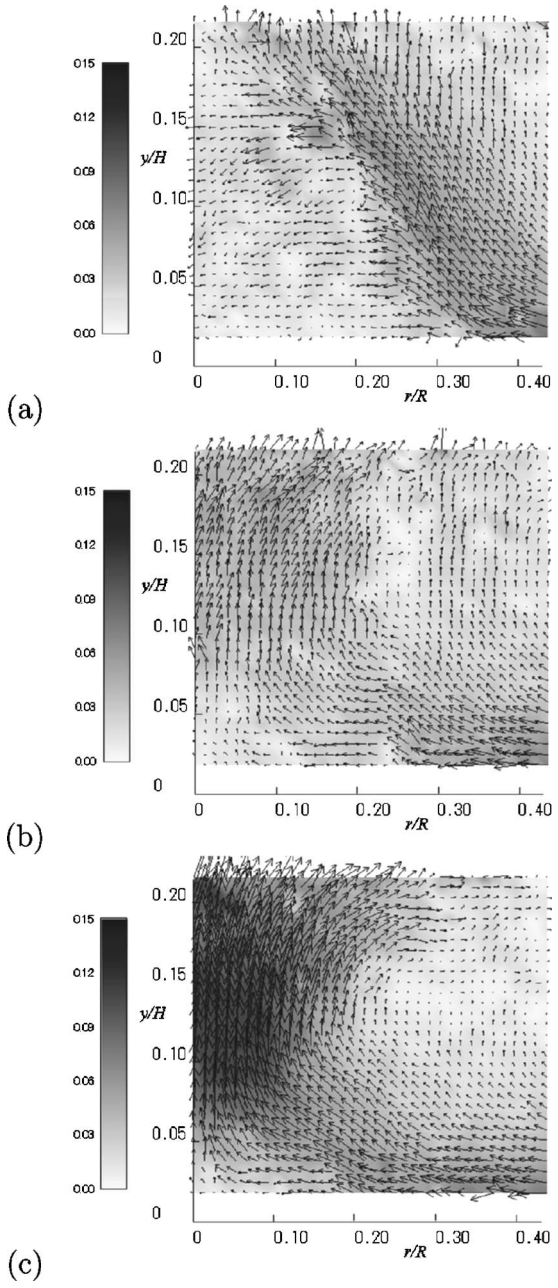

FIG. 5. Velocity vector and contour on the $r-y$ section for PAA 0.5 wt. % at $\mathrm{Re}_0=2.1$, $E_0=14$: (a) $t/T=0.945$, (b) $t/T=1.000$, (c) $t/T=1.024$.

To investigate the difference in velocity fluctuations at two axial locations, $y/H=0.05$ and $y/H=0.08$, axial and radial velocity fluctuations for PAA 0.5 wt. % at $r/R=0.10$, $\mathrm{Re}_0=2.1$ are shown in Figs. 7(a) and 7(b), respectively. At $y/H=0.05$, the axial velocity fluctuation $v_y/(R\Omega)$ is gradually increasing after the vortex shedding $(t/T>1)$, and then at $t/T=1.024$ it becomes a positive maximum which is smaller than that at $y/H=0.08$. The negative radial velocity fluctuations $v_r/(R\Omega)$ at both $y/H=0.05$ and $y/H=0.08$ become slightly larger after the vortex shedding and reach a minimum at $t/T=1.024$. This indicates that the large-scale secondary flow is flowing near the rotating axis through the region close to the rotating disk after the vortex shedding.

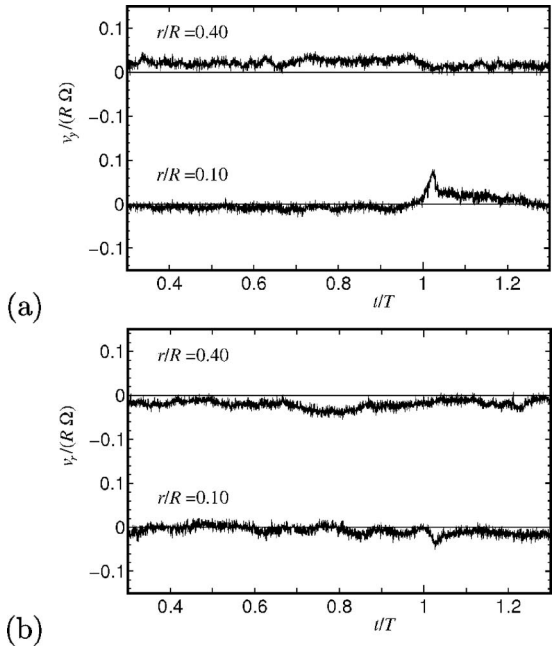

FIG. 6. Velocity fluctuations for PAA 0.5 wt. % at $y/H=0.08$, $\mathrm{Re}_0=2.1$, $E_0=14$: (a) axial, (b) radial.

C. Nonaxisymmetric ring vortex

At the higher Reynolds numbers within the vortex shedding region in the Re_0-E_0 diagram, the ring vortex becomes nonaxisymmetric.[9] Figures 8(a) and 8(b) show the azimuthal and radial velocity fluctuations for PAA 1.0 wt. % at $y/H=0.08$, $\mathrm{Re}_0=1.9$. Figure 8(a) shows that the periodic oscillation of the azimuthal velocity component $v_\theta/(R\Omega)$ is large at $r/R=0.20, 0.30$, but small at $r/R=0.40$. On the other hand, the large amplitude oscillation of the radial velocity component $v_r/(R\Omega)$ is observed at any radial locations examined, as shown in Fig. 8(b). It is noticeable that the azimuthal velocity, which represents the main flow, periodically oscillates with considerably large amplitude. In addition, note that the time variation of radial velocity component for PAA 1.0 wt. % at $r/R=0.30$ has two distinct periods as shown in Fig. 8(b). In Fig. 9, both azimuthal and radial velocity fluctuations for PAA 1.0 wt. % at $y/H=0.08$, $r/R=0.30$, $\mathrm{Re}_0=1.9$ are shown to clarify two distinct periods of $v_r/(R\Omega)$.

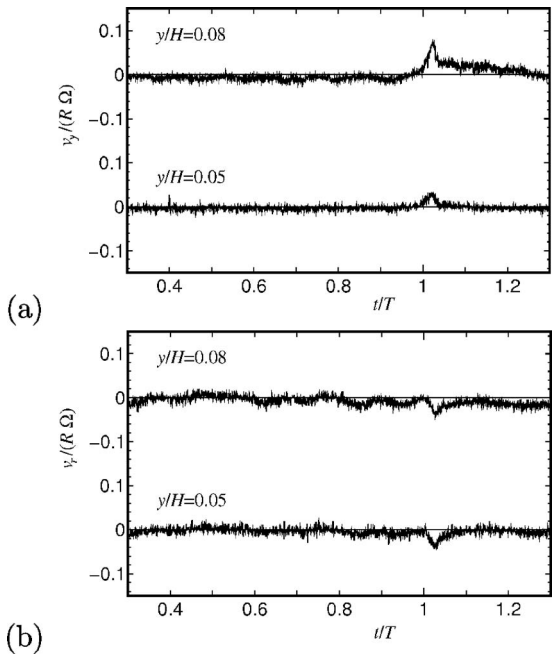

FIG. 7. Velocity fluctuations for PAA 0.5 wt. % at $r/R=0.10$, $\mathrm{Re}_0=2.1$, $E_0=14$: (a) axial, (b) radial.

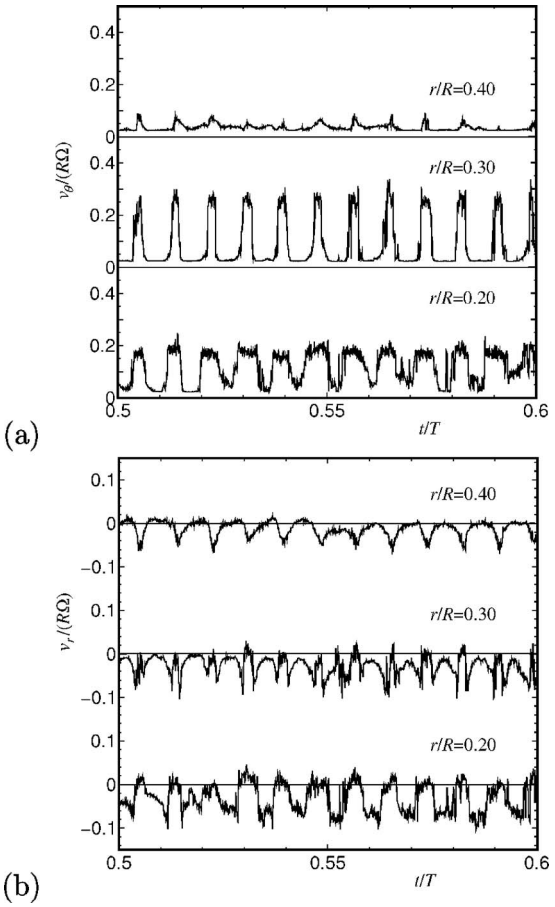

FIG. 8. Velocity fluctuations for PAA 1.0 wt. % at $y/H=0.08$, $\mathrm{Re}_0=1.9$, $E_0=78$: (a) azimuthal, (b) radial.

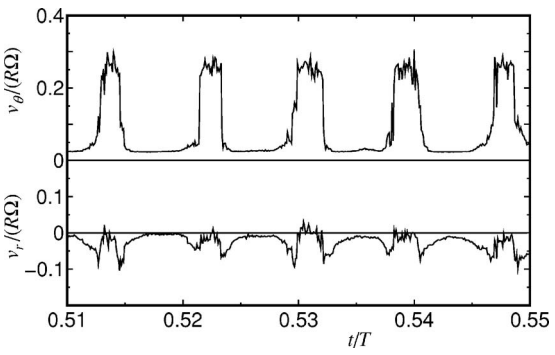

FIG. 9. Azimuthal and radial velocity fluctuations for PAA 1.0 wt. % at $y/H=0.08$, $r/R=0.30$, $\mathrm{Re}_0=1.9$, $E_0=78$.

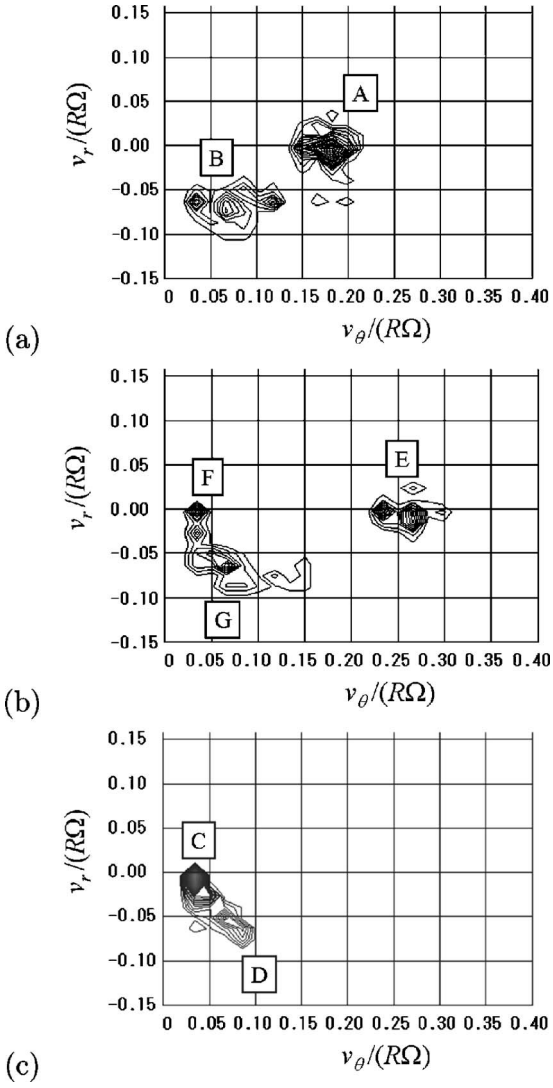

FIG. 10. Joint probability density functions of azimuthal and radial velocity fluctuations for PAA 1.0 wt. % at $y/H=0.08$, $\mathrm{Re}_0=1.9$, $E_0=78$: (a) $r/R=0.20$, (b) $r/R=0.30$, (c) $r/R=0.40$.

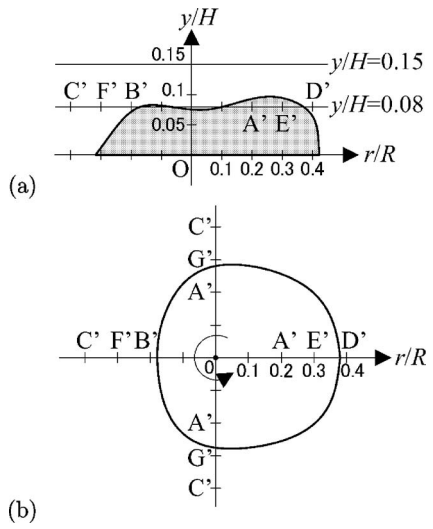

FIG. 11. Outline of nonaxisymmetric ring vortex for PAA 1.0 wt. % at $\mathrm{Re}_0=1.9$, $E_0=78$: (a) $r-y$ section, (b) $r-\theta$ section at $y/H=0.08$.

These new findings are explained by using the joint probability density function (jpdf) and the model of the nonaxisymmetric ring vortex as follows.

Figure 10 shows the jpdf of azimuthal and radial velocity fluctuations for PAA 1.0 wt. % at $y/H=0.08$, $\mathrm{Re}_0=1.9$. Figures 10(a)–10(c) show the jpdf at $r/R=0.20$, $r/R=0.30$, and $r/R=0.40$, respectively. Here, in order to clarify the relation between the locations examined for jpdf and the nonaxisymmetric ring vortex, we show the outline of the nonaxisymmetric ring vortex for PAA 1.0 wt. % at $\mathrm{Re}_0=1.9$ in Fig. 11. Figure 11(a) shows the outline of the nonaxisymmetric ring vortex in the meridian $(r-y)$ section for PAA 1.0 wt. % at $\mathrm{Re}_0=1.9$ in Fig. 11. Figure 11(a) shows the outline of the nonaxisymmetric ring vortex in the meridian $(r-y)$ section for PAA 1.0 wt. % at $\mathrm{Re}_0=1.9$, while Fig. 11(b) presents the outline in the $r-\theta$ section at $y/H=0.08$. Note that in the quasisteady state before the vortex shedding, the nonaxisymmetric ring vortex rotates while retaining its shape as shown in Fig. 11. In Fig. 11, A′ $(r/R=0.2)$ and E′ $(r/R=0.3)$ represent the inside of the nonaxisymmetric ring vortex, while B′ $(r/R=0.2)$, D′ $(r/R=0.4)$, and G′ $(r/R=0.3)$ represent the locations within the high shear layer at the boundary between the nonaxisymmetric ring vortex and its outer large-scale secondary flow; and C′ $(r/R=0.4)$ and F′ $(r/R=0.3)$ represent the locations in the large-scale secondary flow. In this case, it can be deduced that at locations A′ and E′, v_θ is large and $|v_r|$ is small, at locations B′, D′, and G′ that v_θ is small and $|v_r|$ is large $(v_r<0)$, and that at the locations C′ and F′, v_θ is smaller than those of the high shear layer (B′, D′, and G′) and $|v_r|$ is small, according to the mean azimuthal and radial velocity profiles for the axisymmetric ring vortex (see Fig. 3).

As shown in Fig. 10(a), the values of the jpdf at $r/R=0.20$ and $y/H=0.08$ are large both in region A $[0.15<v_\theta/(R\Omega)<0.20$ and $v_r/(R\Omega)\simeq 0]$ and region B $[0.05<v_\theta/(R\Omega)<0.10$ and $-0.10<v_r/(R\Omega)<-0.05]$. Jpdf in region A in Fig. 10(a) represents the value at the location inside the nonaxisymmetric ring vortex (A′ in Fig. 11), while jpdf in region B represents the value at the location within the high shear layer (B′ in Fig. 11). Two kinds of flow situations would occur periodically at the location of $r/R=0.20$ and $y/H=0.08$, so that time oscillations of azimuthal and radial velocity fluctuations with large amplitude appeared (see Fig. 8).

As shown in Fig. 10(b), the values of jpdf at $r/R=0.30$ and $y/H=0.08$ are large in region E $[0.22<v_\theta/(R\Omega)<0.28$ and $v_r/(R\Omega)\simeq 0]$, region F $[0.02<v_\theta/(R\Omega)<0.05$ and $v_r/(R\Omega)\simeq 0]$, and region G $[0.05<v_\theta/(R\Omega)<0.10$ and $-0.10<v_r/(R\Omega)<-0.05]$. This is due to three kinds of flow situations occurring at $r/R=0.30$ and $y/H=0.08$, i.e., flow situations occurring on the inside of the nonaxisymmetric ring vortex (E′ in Fig. 11), on the outside (F′ in Fig. 11), and at the location within the high shear layer (G′ in Fig. 11). When the nonaxisymmetric ring vortex makes one revolution, the measurement location changes as follows: F′ → G′ → E′ → G′ → F′ (Fig. 11). As a result, at $r/R=0.30$ and $y/H=0.08$, the azimuthal velocity v_θ would change to small → small → large → small → small, while the absolute ra-

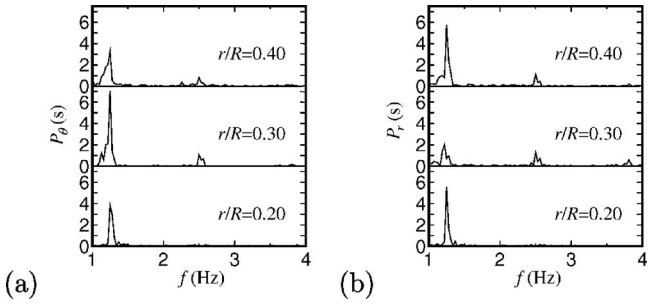

FIG. 12. Power spectra of velocity fluctuations for PAA 1.0 wt. % at $y/H=0.30$, $\mathrm{Re}_0=1.9$, $E_0=78$: (a) azimuthal, (b) radial.

dial velocity $|v_r|$ would change to small→large ($v_r<0$) →small→large ($v_r<0$)→small. Therefore, the time variation of azimuthal velocity component has only a single period, while the time variation of the radial velocity component has a double periodicity for PAA 1.0 wt. % at $r/R=0.30$ and $y/H=0.08$ (see Fig. 9).

Figure 10(c) shows that the values of jpdf at $r/R=0.40$ and $y/H=0.08$ are large in region C $[0.02<v_\theta/(R\Omega)<0.05$ and $v_r/(R\Omega)\simeq 0]$ and region D $[0.05<v_\theta/(R\Omega)<0.10$ and $-0.08<v_r/(R\Omega)<-0.04]$. Jpdf in region C in Fig. 10(c) represents the value at the location outside the nonaxisymmetric ring vortex (C′ in Fig. 11), while jpdf in region D represents the value at the location within the high shear layer (D′ in Fig. 11). Two kinds of flow situations would occur periodically at the location of $r/R=0.40$ and $y/H=0.08$, so that time oscillations of azimuthal and radial velocity fluctuations, which are small and large, respectively, are observed (see Fig. 8).

Next, we investigate the frequency of periodic time oscillations for the azimuthal and radial velocity fluctuations. Figures 12(a) and 12(b) show the power spectra of azimuthal and radial velocity fluctuations (P_θ and P_r) for PAA 1.0 wt. % at $y/H=0.08$, $\mathrm{Re}_0=1.9$, respectively. At any radial location tested, distinct peaks appear at the frequency $f\simeq 1.2$ Hz in the profiles of P_θ and P_r. The nondimensional frequency $f^*=2\pi f/\Omega$ is about 0.8, which indicates that the angular velocity of the nonaxisymmetric ring vortex is about 0.8 times that of the rotating disk. The nondimensional frequency $f^*\simeq 0.8$ is also obtained for PAA 0.5 wt. %, and is supported by the sectional flow visualization. In the profile of P_r at $r/R=0.30$, the second peak at $f\simeq 2.4$ Hz is comparable with the first peak at $f\simeq 1.2$ Hz [Fig. 12(b)]. This is consistent with the double periodicity of radial velocity fluctuation in addition to the harmonics (see Fig. 9). On the other hand, the second peak of P_r at $r/R=0.40$ is attributable to the harmonics, which is confirmed by the time variation of radial velocity fluctuation shown in Fig. 8(b).

To examine the difference in velocity fluctuations between $y/H=0.08$ and $y/H=0.15$, the azimuthal and radial velocity fluctuations for PAA 1.0 wt. % at $r/R=0.30$, $\mathrm{Re}_0=1.9$ are shown in Figs. 13(a) and 13(b), respectively. At $r/R=0.30$, the azimuthal and radial velocity fluctuations at $y/H=0.15$ are almost constant unlike at $y/H=0.08$. This is because at $r/R=0.30$, the location of $y/H=0.08$ becomes

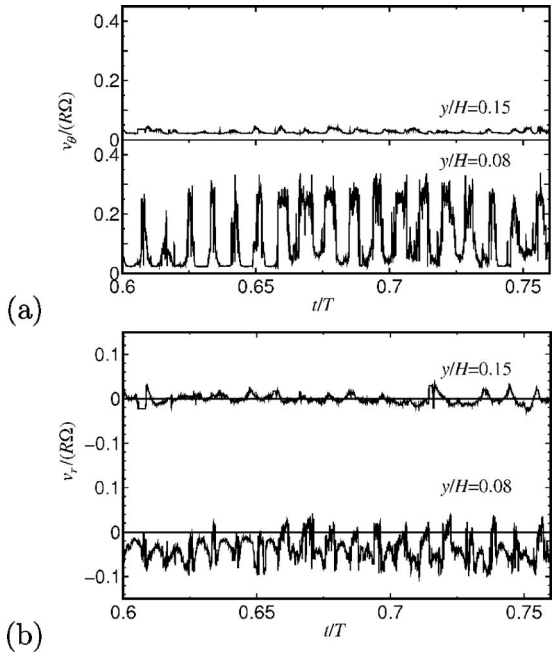

FIG. 13. Velocity fluctuations for PAA 1.0 wt. % at $r/R=0.30$, $\mathrm{Re}_0=1.9$, $E_0=78$: (a) azimuthal, (b) radial.

both the outside and inside of the nonaxisymmetric ring vortex, while the location of $y/H=0.15$ is outside at all times [see Fig. 11(a)].

Velocity measurements for the nonaxisymmetric ring vortex reveal that once the axisymmetric property is broken, the flow fields near the rotating disk become rather complex, in which the correlation between azimuthal and radial velocity fluctuations varies with the radial locations, in addition to quite large periodic oscillations with time.

IV. CONCLUSIONS

Unsteady swirling flows of polyacrylamide solutions in a cylindrical casing with a rotating disk have been investigated by two-dimensional PIV measurements for the meridian $(r-y)$ and $r-\theta$ sections at relatively high Reynolds numbers. The main results of the present study may be summarized as follows:

(1) The fluid within the ring vortex rotates with semirigid rotation, where the angular velocity of the ring vortex is about 0.9 times that of the rotating disk.
(2) A high shear layer exists at the boundary between the ring vortex and the outer large-scale secondary flow, which supports the vortex shedding mechanism based on the elastic energy.
(3) Just after the ring vortex was shed, the surrounding large-scale secondary flow rushed into the area near the rotating axis.
(4) For the nonaxisymmetric ring vortex, azimuthal and radial velocities periodically oscillate with considerably large amplitude, and their correlation varies with the

radial locations. These findings are explained by using the joint probability density function and the model of the nonaxisymmetric ring vortex.

ACKNOWLEDGMENTS

The gear motor with inverter provided by Sumitomo Heavy Industries, Ltd. is gratefully acknowledged. Special thanks are also due to A. Sasakawa, and H. Koshino for their unfailing assistance with the experimental measurements.

[1] C. T. Hill, "Nearly viscometric flow of viscoelastic fluids in the disc and cylinder system. II: Experimental," Trans. Soc. Rheol. **16**, 213 (1972).
[2] C. Day, J. A. Harris, J. Soria, D. V. Boger, and M. C. Welsh, "Behavior of an elastic fluid in cylindrical swirling flow," Exp. Therm. Fluid Sci. **12**, 250 (1996).
[3] M. P. Escudier and L. M. Cullen, "Flow of a shear-thinning liquid in a cylindrical container with a rotating end wall," Exp. Therm. Fluid Sci. **12**, 381 (1996).
[4] T. Moroi, M. Itoh, K. Fujita, and H. Hamasaki, "Viscoelastic flow due to a rotating disc enclosed in a cylindrical casing (Influence of aspect ratio)," JSME Int. J., Ser. B **44**, 465 (2001).
[5] M. Itoh, M. Suzuki, and T. Moroi, "Swirling flow of a viscoelastic fluid in a cylindrical casing," ASME Trans. J. Fluids Eng. **128**, 88 (2006).
[6] J. R. Stokes, L. J. W. Graham, N. J. Lawson, and D. V. Boger, "Swirling flow of viscoelastic fluids. Part 1. Interaction between inertia and elasticity," J. Fluid Mech. **429**, 67 (2001).
[7] J. R. Stokes, L. J. W. Graham, N. J. Lawson, and D. V. Boger, "Swirling flow of viscoelastic fluids. Part 2. Elastic effects," J. Fluid Mech. **429**, 117 (2001).
[8] J. R. Stokes and D. V. Boger, "Mixing of viscous polymer liquids," Phys. Fluids **12**, 1411 (2000).
[9] S. Tamano, M. Itoh, Y. Ide, and K. Yokota, "Vortex shedding in confined swirling flow of polymer solutions," Phys. Fluids **19**, 023103 (2007).
[10] J. N. Sørensen, I. Naumov, and R. Mikkelsen, "Experimental investigation of three-dimensional flow instabilities in a rotating lid-driven cavity," Exp. Fluids **41**, 425 (2006).
[11] J. Wei, F.-C. Li, B. Yu, and Y. Kawaguchi, "Swirling flow of a viscoelastic fluid with free surface-Part 1: Experimental analysis of vortex motion by PIV," ASME Trans. J. Fluids Eng. **128**, 69 (2006).
[12] F.-C. Li, M. Oishi, Y. Kawaguchi, N. Oshima, and M. Oshima, "Experimental study on symmetry breaking in a swirling free-surface cylinder flow influenced by viscoelasticity," Exp. Therm. Fluid Sci. **31**, 237 (2007).